LAWRENCE
LIVERMORE
NATIONAL
LABORATORY

LLNL-JRNL-744427

Deformation of Granular Material under Continuous Principal Stress Axes Rotation

R. Wang, P. Fu, J. M. Zhang, Y. F. Dafalias

January 11, 2018

International Journal of Geomechanics

Disclaimer

Deformation of Granular Material under Continuous Rotation of Stress Principal Axes

Rui Wang[1,2], Pengcheng Fu[3], Jian-Min Zhang[1,2], and Yannis F. Dafalias[4,5]

[1]Department of Hydraulic Engineering, State Key Laboratory of Hydroscience and Engineering, Tsinghua University, Beijing, 100084, China.

[2]National Engineering Laboratory for Green & Safe Construction Technology in Urban Rail Transit, Tsinghua University, Beijing, 100084, China.

[3]Atmospheric, Earth, and Energy Division, Lawrence Livermore National Laboratory, Livermore, CA 94551, USA

[4]Department of Civil and Environmental Engineering, University of California, Davis, CA 95616, U.S.A.

[5]Department of Mechanics, School of Applied Mathematical and Physical Sciences, National Technical University of Athens, Greece.

Abstract

Mechanical responses of granular material to rotation of stress principal axes is an issue of both practical and theoretical importance in soil mechanics. Using 2D DEM (two-dimensional discrete element method) simulation, this study investigates the deformation of granular material under continuous rotation of stress principal axes maintaining the principal stress values fixed. It is shown that under such rotation the deformation can exceed the one caused by fixed principal stress axes cyclic biaxial compression with a maximum deviatoric stress ratio that equals the fixed stress ratio during rotation. The volumetric strain is overall contractive, while oscillating within each load cycle for specimens with significant fabric anisotropy. Initial fabric anisotropy orientation is shown to have little influence on the overall evolution of volumetric strain, while it does affect shear strain development. During the initial stress principal axes rotation cycles, the dilatancy of granular material, in the contractive direction, is dominated by the evolving orientation of major principal stress axis in reference to the initial major principal stress axis during anisotropic consolidation, and

the influence of initial fabric anisotropy orientation is trivial. As stress rotation continues, the influence of the relative orientation between stress and fabric becomes prominent, causing the material to dilate when the major principal stress axis rotates from the normal of the bedding plane to being perpendicular to it, and contract during the other half of the cycle.

Keywords: Granular material; Continuous stress principal axes rotation; Discrete element method; Deformation; Fabric

1 Introduction

Stress in soil under natural and engineering loads (e.g. wave loads, seismic loads, traffic loads etc.) rarely evolve with fixed principal axes (Pyke et al., 1975; Seed et al., 1978; Ishihara and Towhata, 1983; Li, 1996; Chang, 2011; Tong et al., 2014). The rotation of stress principal axes (PA) has been suggested to significantly influence the mechanical response of soil, increasing deformation and reducing liquefaction resistance, compared with loading involving only stress magnitude variation along fixed principal axes (Seed et al., 1978; Arthur et al., 1979; Ishihara and Yamazaki, 1980; Tokimatsu and Yoshimi, 1982; Towhata and Ishihara, 1985) even when the magnitudes of principal stresses in the two scenarios are the same.

Laboratory experiments (Arthur et al., 1977; Hight et al., 1983; Matsuoka et al., 1985; Miura et al., 1986 a, b; Symes et al., 1988; Vaid et al., 1990; Wijewickreme and Vaid, 1993; Yang et al., 2007; Tong et al., 2010; Jiang et al. 2013; Cai et al., 2013) and DEM (Discrete Element Method, Cundall and Strack, 1979) numerical simulations (Tsutsumi and Kaneko 2008; Jiang et al., 2006; Li and Yu, 2010; Tong et al., 2014; Wan and Hadda, 2015; Theocharis et al., 2017) have been conducted to study soil behavior under continuous stress PA rotation. Since Ishihara and Towhata (1983) pointed out that the strain increment direction does not align with the stress direction during stress PA rotation, this phenomenon has become a major focus in studies concerning stress PA rotation. The non-coaxiality between strain increment and stress has been analyzed in detail (Miura et al., 1986 a, b; Gutierrez et al., 1991; Cai et al., 2013; Tong et al., 2014; Xiong et al., 2015; Yan et al., 2015). For example, Gutierrez et al. (1991) studied the

dependency of plastic strain increment direction on the stress increment direction through a series of well-designed stress PA rotation and probe tests. These advances have been utilized as explanations for the deformation of soil under principal stress rotation in constitutive modeling efforts (Prandel et al., 1990; Gutierrez et al., 1993; Lashkari and Latifi, 2008; Yang and Yu, 2013). Nevertheless, as important as it is, this non-coaxiality is only one specific aspect of the loading scheme of soils under stress PA rotation (Tejchman and Wu, 2009), and should not be considered the sole or main fundamental cause for the deformation behavior of soil under such stress path. More recently, constitutive modeling efforts have been made to take into consideration the effect of stress PA rotation through incorporating intrinsic and fundamental soil properties, particularly fabric anisotropy (e.g. Li and Dafalias, 2004; Iai et al., 2003; Taha and Shaverdi, 2014, Yao et al., 2017).

Although existing experimental results have addressed some aspects of the deformation of soil under stress PA rotation (Miura et al., 1986; Tong et al., 2010; Xiong et al., 2015), more comprehensive and extensive study is still needed to investigate the behavior of soil deformation characteristics during stress PA rotation, including volumetric strain, shear strain, and dilatancy (the relationship between volume change and shear deformation). Such studies would enhance rational understanding of the fundamental characteristics of soil deformation under stress PA rotation, and furthermore they will enhance the basic understanding of the fundamental mechanism that defines dilatancy whose understanding and analytical description so far seems to have been restricted to monotonic radial (and co-axial) loading conditions.

82 Recent developments in numerical simulation technologies has offered a powerful
83 tool for the study of soil behavior under complex loading such as stress PA rotation,
84 providing access to grain scale fabric information. Since Thornton's (2000) pioneering
85 numerical study of granular media under complex three-dimensional loading, DEM has
86 been increasingly utilized to analyze granular material under stress PA rotation (e.g. Li
87 and Yu, 2010; Tong et al (2014); Theocharis et al., 2017). However, the connection
88 between fabric evolution and soil deformation during continuous stress PA rotation still
89 needs to be further studied to properly test the long-existing hypothesis that the
90 deformation of granular material under stress PA rotation is caused by anisotropy of the
91 material (Li and Dafalias, 2004; Iai et al., 2003; Taha and Shaverdi, 2014).
92 The current study aims to address the aforementioned needs by conducting an in-
93 depth analysis of deformation patterns of granular material and the connection between
94 fabric evolution and deformation of granular material under continuous stress PA
95 rotation. In this work, such rotation refers to the process in which the stress principal
96 axes rotate continuously for a considerable number of cycles without any change in the
97 principal stress magnitudes and rotation direction (i.e. clockwise or counterclockwise),
98 and is abbreviated as "stress rotation". A load cycle is complete when the principal
99 stress rotates by 180° due to symmetry. This continuous stress rotation is the simplest
100 and most fundamental form of stress PA rotation, and has been identified as the stress
101 path induced in soil by waves load on seabed (Ishihara and Towhata, 1983), an issue of
102 great practical values for seabed foundation geotechnical engineering. The simulation
103 method and program adopted in this study are presented in Section 2. Typical

deformation development and fabric evolution results during stress rotation are presented in Section 3, including one case of deformation caused by cyclic biaxial loading of same deviatoric stress amplitude. The volumetric strain, shear strain, and dilatancy under stress rotation is analyzed in sections 4 to 6, respectively, with special focus on the role of fabric anisotropy. The influence of initial fabric anisotropy intensity and loading history is discussed in section 7.

2 DEM simulation program

2.1 Simulation method

2D DEM simulations of elliptical particles are conducted in this study to investigate the deformation of granular materials under stress rotation using *PPDEM* (Polyarc Parallel-processing Discrete Element Modeling, Fu et al. 2012). 3D granular materials and 2D particle-based models behave differently in certain aspects. For instance, 2D particle assemblies generally have lower void ratio and coordination numbers than their 3D counterparts. However, 2D DEM's ability to quantify, in high fidelity, grain-scale processes and qualitatively predict granular material behavior, including previously unknown behavior has been proven by numerous studies, including prior applications of the *PPDEM* code (e.g. Fu and Dafalias, 2011 a, b; Tong et al, 2014; Fu and Dafalias, 2015; Wang et al, 2016; Wang et al 2017, a, b). Moreover, *PPDEM*'s parallel computation capability makes the long-duration simulations (involving many loading cycles) conducted in this study computationally tractable, which amounted to over 5000 core-hours on Intel Xeon E5-2697 CPUs.

A total of 16 DEM simulations are conducted in this study, including 15 stress rotation simulations, and one cyclic biaxial simulation with fixed principal stress axes,

as listed in Table 1. The naming convention for the simulation IDs reflects important characteristics of each simulation. The first letter in the simulation ID represents the density of the specimen, L stands for relatively loose, D stands for relatively dense, and M stands for medium. The second letter represents the fabrication method of the specimen, G stands for gravity deposition, C stands for centripetal acceleration, and R means the specimen is reconsolidated from a previous specimen that has experienced certain load histories. The first number following the letters indicates the deviatoric stress magnitude in kPa. The second number, if applicable, is the initial bedding plane orientation in degrees relative to the horizontal plane. CB at the end of the ID indicates that the simulation is a cyclic biaxial with fixed PSA.

Table 1. Continuous cyclic principal stress rotation simulation program

ID	e_{in}	Fabrication method	q (kPa)	Ψ (°)	α_{cin}	α_{pin}
DG-25-0	0.1818	gravity deposition	25	0	0.075	0.126
DG-0	0.1821	gravity deposition	0	0	0.057	0.127
DG-25-0-CB	0.1818	gravity deposition	25	0	0.075	0.126
DG-25-30	0.1817	gravity deposition	25	30	0.069	0.125
DG-25-60	0.182	gravity deposition	25	60	0.043	0.128
DG-25-90	0.1819	gravity deposition	25	90	0.022	0.126
DG-10-0	0.1819	gravity deposition	10	0	0.062	0.126
DG-40-0	0.182	gravity deposition	40	0	0.102	0.124
LG-25-0	0.2172	gravity deposition	25	0	0.135	0.218
LG-25-30	0.217	gravity deposition	25	30	0.126	0.217
LG-25-60	0.2168	gravity deposition	25	60	0.101	0.216
LG-25-90	0.2162	gravity deposition	25	90	0.076	0.221
LG-10-0	0.2174	gravity deposition	10	0	0.123	0.216
LG-40-0	0.2165	gravity deposition	40	0	0.155	0.219
DC-25	0.1819	centripetal acceleration	25	/	0.024	0.008
MR-25	0.1964	reconstructed from LG-25-0	25	/	0.071	0.119

Note: The initial void ratio e_{in}, contact normal fabric anisotropy intensity α_{cin}, and particle orientation fabric anisotropy intensity α_{pin} are measured after consolidation under deviatoric stress.

The cyclic biaxial simulation DG-25-0-CB provides a comparison baseline for the deformation of granular material under principal stress rotation. A simulation DG-0, in which the applied isotropic stress is numerically rotated, is conducted to validate the

algorithm of applying rotating stress boundary conditions. Among the other 14 principal stress rotation simulations, the influences of initial void ratio (e_{in}), initial fabric anisotropy, deviatoric stress ratio (η), and stress history are investigated. Two series of stress rotation simulations on specimens with different initial void ratios are conducted, namely the DG and LG series. Within each series, variations in initial fabric anisotropy orientation is achieved by altering the initial bedding plane angle ψ, i.e. the angle between the bedding plane and the horizontal plane (Fig. 1). Simulations under three different deviatoric stress levels are also conducted within each of the DG and LG series. The influence of initial fabric anisotropy intensity is evaluated through comparison of the DG series with a simulation on an initially isotropic specimen (DC-25-0). The influence of loading history is isolated and investigated using a specimen that had undergone previous loading (MR-25) to achieve approximately the same initial fabric anisotropy as that of DG-25-0. All the simulations in this study are conducted under a mean effective stress of 125 kPa. Note, the unit of stress in 2D is expressed in per meter (out-of-the-plane direction) terms in this study to be consistent with the conventional stress unit of kPa.

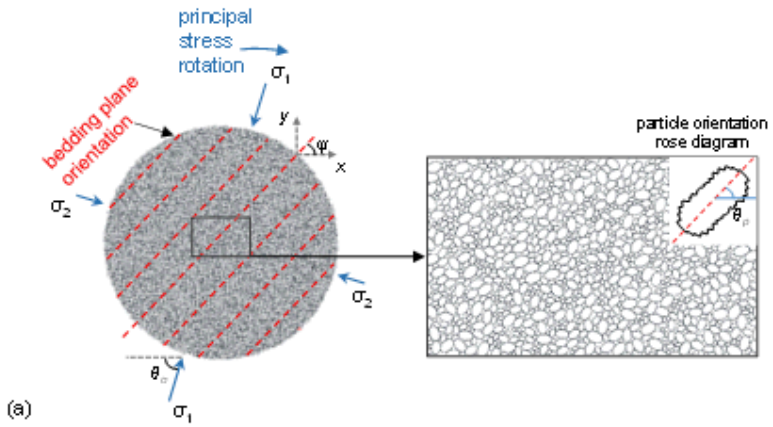

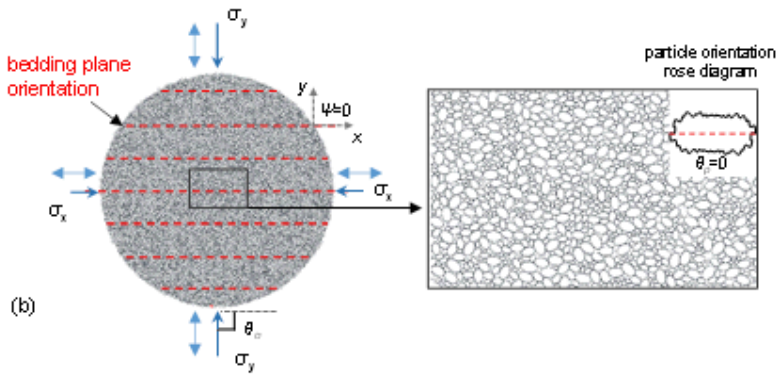

Fig. 1. Schematic diagram of the loading of specimens: (a) stress principal axes rotation applied on a specimen with an initial bedding plane angle of ψ; (b) cyclic biaxial loading. Both specimens are circular in shape, cut out from the granular material, and then consolidated to the initial stress state.

Initially anisotropic granular material is fabricated by pluviating 100,000 randomly generated elliptical particles under gravity following procedures presented by Fu and Dafalias (2011 a), whereas the initially isotropic specimen (DC-25) is fabricated by applying centripetal acceleration to 100,000 particles with a uniform distribution of original orientations. The method of fabricating initially isotropic granular material under centripetal acceleration has been proved successful in achieving an isotropic initial state by Wang et al. (2017 b). The homogeneity of the fabricated material is checked carefully following the procedures of Fu and Dafalias (2011 a). Circular specimens (Fig. 1) consisting of approximately 15,000 particles each are then cut out from the fabricated anisotropic and isotropic materials, with the circular shape of the specimen chosen for the convenience of the homogeneous application of the stress boundary condition during principal stress rotation.

Stress boundary condition with arbitrary principal values and orientations is achieved following a method of applying distributed forces along the principal stress directions directly to boundary particles proposed by Tong et al (2014), guaranteeing the homogeneity of the applied stress and the free deformation of the specimen. In this

paper, the orientation of the major principal stress axes $\theta_{\sigma 1}$ is referred to as the angle between the current major principal stress axis and the horizontal direction (Fig. 1). The circular specimens cut out from the virtual granular material are first rotated to the designated initial bedding plane angle ψ (Fig. 1), and then consolidated under the desired stress state before rotational loading. At the initiation of stress rotation, the major principal stress orientation coincides with the vertical direction (y axis), and the minor principal stress orientation coincides with the horizontal direction (x axis), i.e. $\sigma_y=\sigma_1$ and $\sigma_x=\sigma_2$. During stress rotation loading, the applied stress, with magnitudes of principal components fixed, is rotated clockwise continuously in a quasi-static state until termination of the simulation when the void ratio of the specimens reaches a relatively steady value (after 60~100 cycles), maintaining the two principal stress values fixed. Other stress paths including biaxial loading with fixed principal stress axes, as in simulation LG-25-0-CB, can also be easily achieved using the boundary stress application method (Fig. 1 (b)).

The virtual granular material used consists of elliptical particles with an aspect ratio of 1.5:1, D_{min}= 0.3mm, D_{max}= 1.0mm, D_{50}= 0.72mm, and inter-particle friction angle of 35°. The elliptical particle shape makes it easy to obtain significant inherent fabric anisotropy through the fabrication process. The inter-particle contact law by Fu and Dafalias (2011 a) is adopted, where the normal force between two contacting particles is proportional to the overlap area. The contact normal stiffness parameter (K_n) is 500 GPa/m (force/overlap area/unit thickness), and the tangential stiffness parameter K_s= 1/3 K_n. See Fu et al. (2012) for a detailed description of the contact law including the

treatment of a minor thermodynamic inconsistency associated with this class of contact law as discovered by Elata and Berrman (1996). The efficacy of the DEM code, simulation method, and contact model have been proved by Tong et al. (2014) in validations against stress rotation laboratory test results on actual sand.

2.2 Stress, strain, and fabric measurement

The stress within the DEM specimens is calculated as (Bagi 1996):

$$\sigma_{ij} = \frac{1}{S}\sum_{k=1}^{N_c} f_i^k l_j^k \tag{1}$$

where S is the area (2D) of the measuring domain; k is an index that runs over all the inter-particle contact points, and N_c is the total number of contacts; f_i^k is the i-component of the k^{th} contact force; l_i^k is the i-component of the branch vector connecting the centers of the two particles of the k^{th} contact. In this study, the stress is measured within the center portion of the circular specimens with more than 10,000 particles, which along with quasi-static loading state guarantees Eq. (1) complies with the uniformity assumptions (Caillerie, 1991) and that secondary terms of the calculated stress tensor are negligible. The deviatoric stress can then defined as $q = (\sigma_1-\sigma_2)/2$, and mean stress $p = (\sigma_1+\sigma_2)/2$.

Local strain in DEM can be inferred from deformation of a reference triangle with vertices attached to the centers of three reference particles, based on a method proposed by Fu and Dafalias (2011 b). The average strains of the specimens are measured with a Delaunay triangulation within the center portion of the circular specimens. Thus, errors caused the occasional large displacement of individual particles at the boundary of the specimen are avoided. In this study, compressive stress and strain are denoted as

positive, following soil mechanics sign conventions.

The second-order contact normal and particle orientation fabric tensors provide information on the fabric anisotropy orientation and intensity of the material. These fabric tensors can unveil important characteristics of granular material relating to its response to principal stress rotation, and can be calculated based on the following general formulation (Satake 1982):

$$\mathbf{F} = \frac{1}{N}\sum_{k=1}^{N} \mathbf{v}^k \otimes \mathbf{v}^k \tag{2}$$

where N is the number of inter-particle contacts or particles in the measuring domain, $\otimes$ denotes tensor product, and the superscript k is the k^{th} contact or k^{th} particle in the measuring domain. When the directional entity $\mathbf{v}$ is the unit contact normal orientation vector $\mathbf{v}_c$, the contact normal fabric tensor $\mathbf{F}_c$ is obtained; when it is the unit particle orientation vector $\mathbf{v}_p$, the particle orientation fabric tensor $\mathbf{F}_p$ is obtained. The measuring domains for the fabric tensors are consistent with those of stress and strain measurements. A fabric tensor in 2D can be uniquely determined by the "intensity" of the anisotropy and the orientation of the fabric, as the trace of the tensor is always unity. The intensity of the anisotropy is the difference between the major and minor principal components of a fabric tensor, or $\alpha=F_1-F_2$, and the orientation of the fabric tensor can be depicted by its major principal direction θ.

3 Typical results

To verify the efficacy of the simulation method and highlight the significance of the granular materials' deformation under stress rotation, the simulation results from DG-25-0 and DG-25-0-CB are first compared in this section. These two simulations have

identical initial conditions and experience the same amplitude of deviatoric stress (q=25 kPa), but are subjected to different loading modes, i.e. stress rotation vs. cyclic biaxial compression. Fig. 2 depicts the stress path of these two simulations, based on actually "measured" stresses according to equation (1), in the p-q space and the τ_{xy}-σ_x space. In the p-q space, the stress path of DG-25-0-CB follows a vertical line with oscillating q and constant p, while that of DG-25-0 is only a single dot, indicating that the principal stress values in DG-25-0 remains constant. In the τ_{xy}-σ_x space, the stress path of DG-25-0-CB follows a horizontal line with no shear stress in the x-y plane, while that of DG-25-0 forms a full circle, indicating the continuous rotation of the principal stress axes. These results show that the adopted simulation method is effective in achieving the target stress paths in high fidelity.

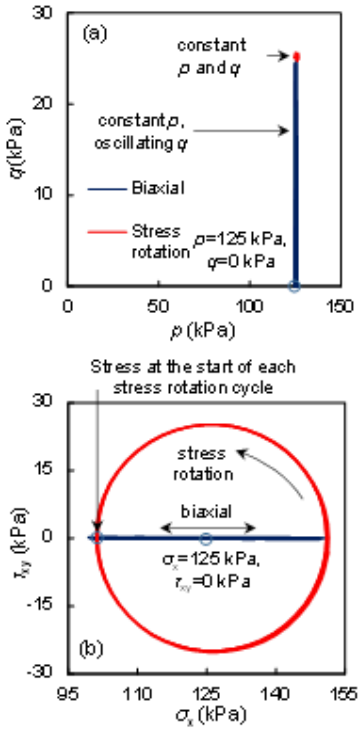

Fig. 2. Measured stress path in DEM simulations for continuous cyclic principal stress rotation (DG-25-0) and cyclic biaxial loading (DG-25-0-CB): (a) stress path in p-q space; (b) stress path in σ_x-τ_{xy} space. Stress paths in 100 cycles of stress rotation and 100 cycles of biaxial loading are

superimposed.

The deformation caused by stress rotation in simulations DG-25-0, and that caused by cyclic loading with fixed principal stress axes in simulation DG-25-0-CB are presented in Fig. 3, along with that of the validation simulation DG-0 subjected to isotropic stress rotation. The strains presented in Fig. 3 include the strains in the x-y coordinate system (ε_x, ε_y, and γ_{xy}), the maximum in-plane shear strain ($\gamma = ((\varepsilon_x - \varepsilon_y)^2 + \gamma_{xy}^2)^{1/2} = (2\mathbf{e}:\mathbf{e})^{1/2}$, $\mathbf{e}$ being the deviatoric strain tensor), and the volumetric strain (ε_v). In both simulations DG-25-0 and DG-25-0-CB, the strains accumulate as stress rotation progresses until gradually reaching their respective steady levels, and the specimen experiences overall contraction during loading. However, for these two simulations with exactly the same initial states, stress rotation induces larger strains than biaxial loading does. For example, the eventual volumetric strain in simulation DG-25-0 oscillates around 0.9%, while that of DG-25-0-CB oscillates around 0.5%. The oscillation amplitude in the former is greater than that of cyclic biaxial loading, apparent in the close-up views shown in Fig. 3 (b) and (f). These results suggest that deformation caused by stress rotation can be very significant for granular materials, and is at least comparable in magnitude to that caused by cyclic biaxial loading. Hence, inadequate consideration for principal stress rotation may cause significant underestimation of soil deformation under many natural and engineering loading scenarios. The results from simulation DG-0 where no discernible deformation occurs during the rotation of the applied isotropic stress (Fig. 3 (c) and (d)) provide verification that the deformation observed due to principal stress rotation in this study is not an artifact induced by the adopted simulation method.

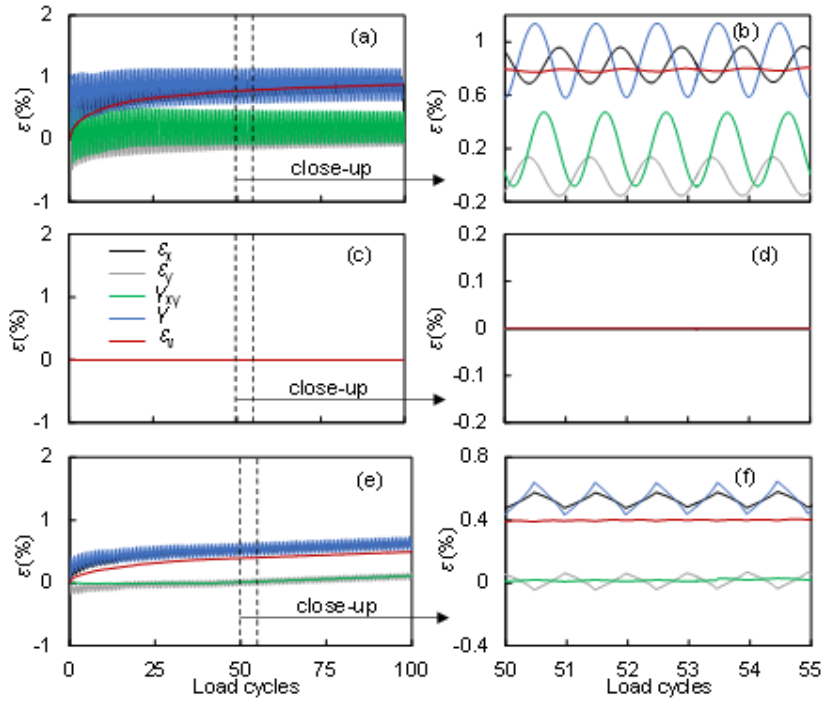

Fig. 3. Strains in simulations: (a) DG-25-0 during 0~100 load cycles, (b) close-up of DG-25-0 during 50~55 load cycles, (c) DG-0 during 0~100 load cycles, (d) close-up of DG-0 during 50~55 load cycles, (e) DG-25-0-CB during 0~100 load cycles, and (f) close-up of DG-25-0-CB during 50~55 load cycles. Five strain components are shown, including normal strain ε_x and ε_y, engineering shear strain γ_{xy}, maximum in-plane engineering shear strain γ, and volumetric strain ε_v.

Fig. 4 shows the rose diagrams for initial contact normal and particle orientation for simulations DG-25-0, DG-25-30, DG-25-60, and DG-25-90 after anisotropic consolidation and immediately before principal stress rotation. These four simulations use the same circular specimen cut out from the gravity-deposited granular material, with the specimen rotated to have initial bedding plane angles of 0°, 30°, 60°, and 90°, respectively. The rose diagrams for the specimen under isotropic stress (p=125 kPa) are also shown as a comparison baseline (Fig. 4 (e)). During consolidation under anisotropic stress (p=125 kPa, q=25 kPa in these four simulations), the contact normal fabric is observed to experience notable changes, which is a characteristic that the anisotropic stress imposes on the material. In general, consolidation under the anisotropic stress induces a contact normal fabric increment in the same direction as

the anisotropic stress. This results in the specimen consolidated under anisotropic stress with initial bedding plane angle $\psi = 0°$ having greater contact normal fabric anisotropy intensity, and the specimen with $\psi = 90°$ having a smaller contact normal fabric anisotropy intensity, compared with the specimen under isotropic stress state. The influence of the changes induced by the anisotropic consolidation stress on the deformation of the specimens is discussed in later sections. In contrast to the contact normal fabric, the particle orientation fabric remains largely unchanged during consolidation, with the only difference among the four being the initial orientation of the fabric, which is within ±2.1° of the bedding plane angle (i.e. $\theta_{p0} \approx \psi$). This difference in the evolution of various fabric tensors under anisotropic biaxial stress has been attributed to the difference in the restriction of each fabric measurement by the geometrical configurations of the granular system in a previous study by Wang et al. (2017 b).

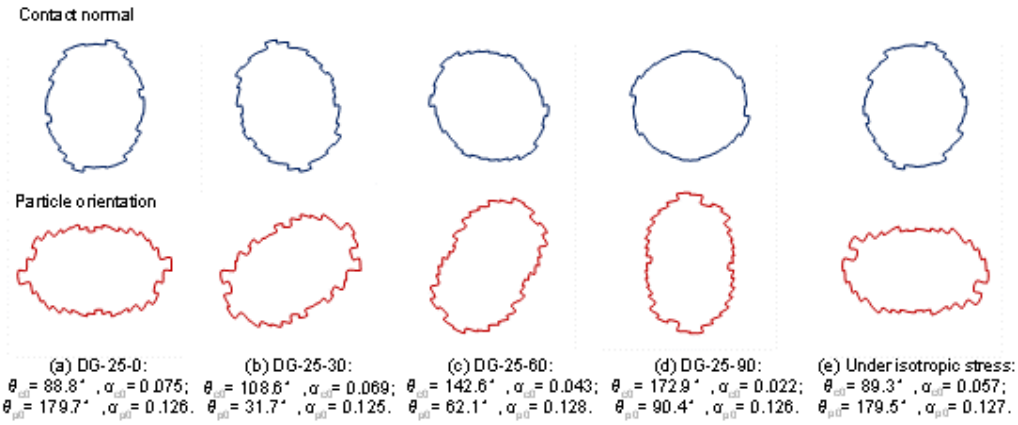

Fig. 4. Initial contact normal and particle orientation fabric rose diagram in simulation series DG. (The numbers 0, 30, 60, and 90 in the simulation IDs represent the initial bedding plane angle of each specimen)

During stress rotation, the intensity of contact normal fabric anisotropy α_c oscillates between approximately 0.025 and 0.070 in all four simulations (Fig. 5 (a) and (b)),

which is close to the range of the initial α_{c0} values of among the four simulations (α_{c0}=0.22 in DG-25-90 and 0.075 in DG-25-0). The contact normal fabric orientation θ_c oscillates within approximately ±10° of each specimen's respective initial contact normal fabric orientation θ_{c0} (Fig. 5 (c) and (d)). In comparison with the contact normal fabric, the particle orientation fabric shows minimal change during principal stress rotation, in terms of both fabric anisotropy intensity and orientation (Fig. 5 (e)~(h)). The variation of particle orientation fabric anisotropy intensity α_p are all within ±0.005 of the initial value, or less than 4% of the initial values. The particle orientation fabric orientation θ_p only deviate from its initial orientation θ_{p0} within ±1.0°. These observed differences in the evolution of the particle orientation fabric and contact normal fabric are attributed to the fact that contact normal is much easier to adjust to external loading, while particle orientation is more strongly constrained by the geometrical arrangement of the granular assembly, unless very large deformation permits significant particle rotations (Fu and Dafalias, 2011a).

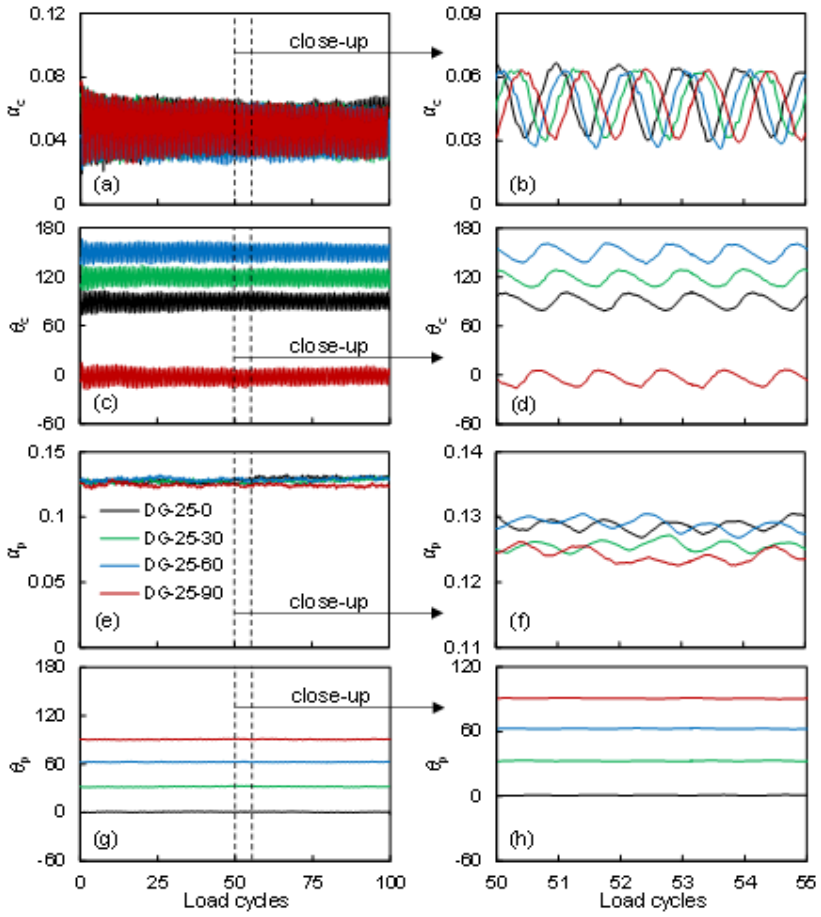

Fig. 5. Evolution of contact normal and particle orientation fabrics during continuous cyclic principal stress rotation in simulation series DG: (a) Contact normal fabric anisotropy intensity αc during 0~100 load cycles, (b) close-up of contact normal fabric anisotropy intensity αc during 50~55 load cycles, (c) major principal contact normal fabric orientation θ_c during 0~100 load cycles, (d) close-up of major principal contact normal fabric orientation θ_c during 50~55 load cycles, (e) particle orientation fabric anisotropy intensity αp during 0~100 load cycles, (f) close-up of particle orientation fabric anisotropy intensity αp during 50~55 load cycles, (g) major principal particle orientation fabric orientation θ_p during 0~100 load cycles, and (h) close-up of major principal particle orientation fabric orientation θ_p during 50~55 load cycles.

4 Volumetric and shear strains under principal stress rotation

The volumetric strain during stress rotation in simulation series DG (DG-25-0, DG-25-30, DG-25-60, and DG-25-90) and LG (the lower density counterparts, namely LG-25-0, LG-25-30, LG-25-60, and LG-25-90) are plotted in Fig. 6, to analyse the influence of initial fabric orientation and void ratio on volumetric strain development. The ultimate steady volumetric strains in the four DG series simulations are very similar,

ranging between 0.83% and 0.89% on the contractive side. The overall volumetric strain evolution in the LG series also appears to be largely independent of the initial fabric orientation, with the ultimate volumetric strains of the four simulations within 1.94%-2.14%. This is reasonable as the initial difference in fabric, which is in terms of the orientation or rotation from a common state, becomes insignificant during many cycles of stress rotations. However, it is somewhat surprising that even during the initial loading cycles, there seems to be no discernible difference in the volumetric strain within each simulation series (Fig. 4 (d)), suggesting that the initial fabric orientation has little influence on the development of volumetric strain. These observations will be discussed in more detail in correlation with dilatancy in Section 5. The volumetric strain in the looser LG series experiences more than twice the contraction of the denser DG series, suggesting that the contractive volumetric strain increases with decreasing relative density.

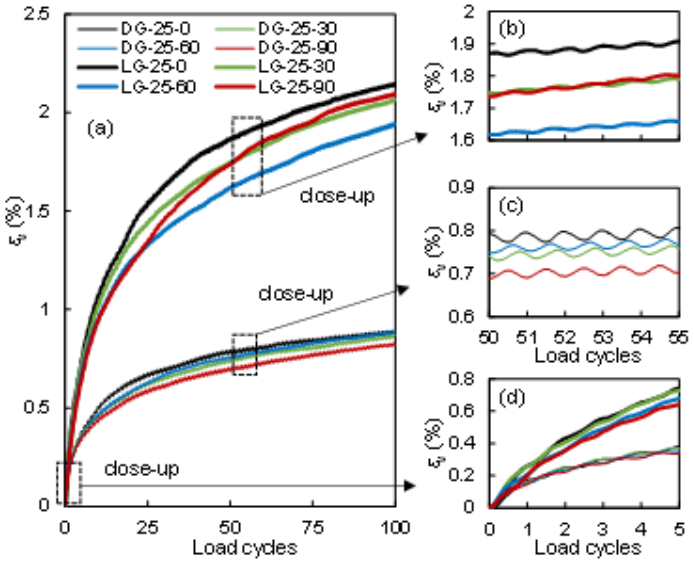

Fig. 6. Volumetric strain during continuous cyclic principal stress rotation in: (a) simulation series DG and LG during 0~100 load cycles, (b) simulation series LG during 50~55 load cycles, (c) simulation series DG during 50~55 load cycles; (d) simulation series DG and LG during 0~5 load

cycles. (D and L represent dense and loose, respectively)

The volumetric strain of DG-40-0, DG-25-0, and DG-10-0 are plotted in Fig. 7 (a), and that of LG-40-0, LG-25-0, and LG-10-0 are plotted in Fig. 7 (b), to analyze the influence of deviatoric stress on volumetric strain. For both the DG and LG series, as the deviatoric stress increases, the contractive volumetric strain increases. For example, the final volumetric strain in DG-40-0 is 1.99%, while that of DG-10-0 is only 0.11%. This naturally raises a question: Will granular material contract or dilate under principal stress rotation when the stress state is above the dilatancy line in the p-q space? During monotonic loading, a material changes from contractive to dilative when it crosses the dilatancy line. In order to answer this question, monotonic biaxial loading with constant p = 125 kPa is applied to the specimen used in both the DG and LG series with initial bedding plane angle of 0°, starting from an isotropically consolidated state. The shear strain γ and volumetric strain ε_v during loading are shown against the deviatoric stress q in Fig. 8, where the q values when the stress rotation begun are also annotated. The peak q for the two specimens under monotonic biaxial loading are 62kPa and 53KPa, respectively (Fig. 8 (a)). The specimen in the DG series with initial bedding plane angle of 0° begins to dilate when the deviatoric stress q exceeds 30kPa (Fig. 8 (b)). This means that even though the DG-40-0 simulation is in a stress state that is above the dilatancy line, the volumetric strain induced by principal stress rotation is still contractive. These results suggest that the overall volumetric strain is always contractive under stress rotation, at least for a 2D case, and the magnitude of contraction increases with increasing deviatoric stress, irrespective of whether or not the stress state is above the dilatancy line.

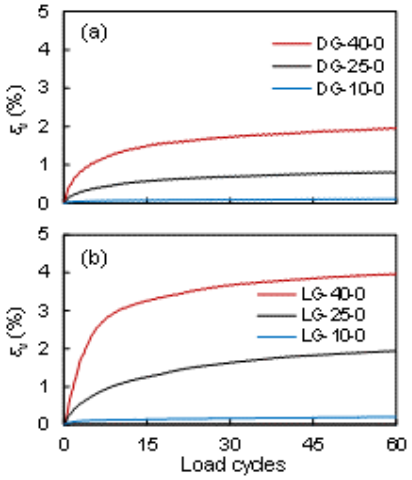

Fig. 7. Influence of deviatoric stress on volumetric strain: (a) DG series, (b) LG series. (The numbers 40, 25, and 10 in the simulation IDs represent the deviatoric stress q in the simulations)

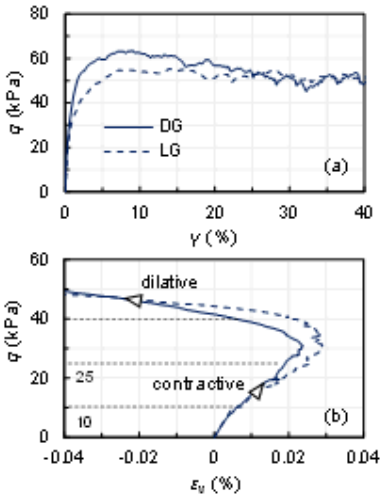

Fig. 8. Volumetric strain under monotonic biaxial loading with constant p = 125kPa in the specimen used in the DG series with initial bedding plane angle of 0°.

Apart from the volumetric strain, another important aspect of the deformation of granular material under stress rotation is the shear strain. The maximum in-plane shear strain γ in the DG series of simulations with varying bedding plane angles (DG-25-0, DG-25-30, DG-25-60, and DG-25-90) are plotted in Fig. 9 (a) and (b). γ oscillates at a largely constant amplitude during loading. The ultimate γ oscillates around values which decrease from 0.8% to 0.3% as the bedding plane angle increases from 0° to 90°. The orientation of the major principal strain $\theta_{\varepsilon 1}$ is plotted in Fig. 9 (c) and (d), which is

at a 45° angle with the normal of the plane that γ occur and can uniquely reflect the orientation of the maximum in-plane shear strain. The orientation $\theta_{\varepsilon 1}$ in the DG series show some limited variation in accordance to the variation of bedding plane angle, all oscillating within ±30° the horizontal direction.

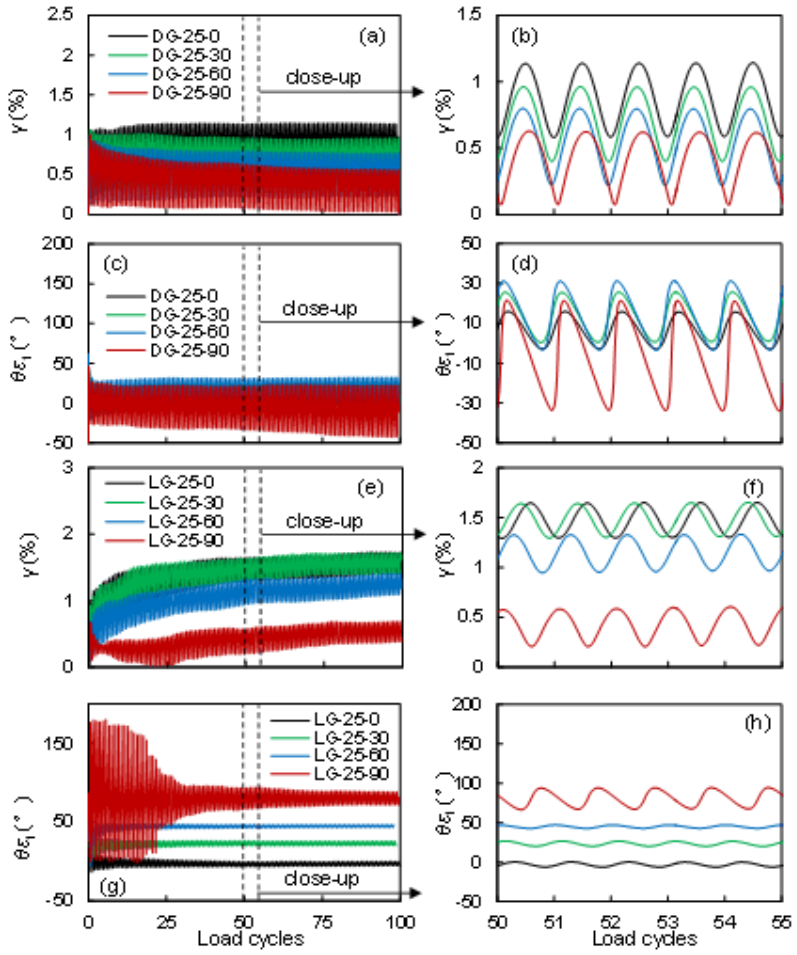

Fig. 9. Evolution of shear strain: (a) maximum shear strain in simulation series DG during 0~100 load cycles, (b) close-up of maximum shear strain in simulation series DG during 50-55 load cycles, (c) orientation of principal strain (45° from the orientation of maximum shear strain) in simulation series DG during 0~100 load cycles, (d) close-up of orientation of principal strain in simulation series DG during 50~55 load cycles, (e) maximum shear strain in simulation series LG during 0~100 load cycles, (f) close-up of maximum shear strain in simulation series LG during 50-55 load cycles, (g) orientation of principal strain in simulation series LG during 0~100 load cycles, (h) close-up of orientation of principal strain in simulation series LG during 50~55 load cycles.

For each simulation in the LG series (LG-25-0, LG-25-30, LG-25-60, and LG-25-90), γ_{max} increases gradually during loading and oscillates around a stabilized value

418 after about 40 cycles, (Fig. 9 (e) and (f)), which is significantly later than their DG
419 counterparts. Similar to the DG series, the ultimate γ also oscillates around values that
420 decrease as the bedding plane angle increases, though the difference between the
421 stabilized γ is more significant, ranging between 0.5% and 1.5%. In contrast to the DG
422 series, $\theta_{\varepsilon 1}$ in the LG series has a clear correspondence with the bedding plane angle,
423 with the eventual $\theta_{\varepsilon 1}$ oscillating around values approximately equal to the bedding plane
424 angle (Fig. 9 (g) and (h)). The amplitude of oscillation of $\theta_{\varepsilon 1}$ in the LG is also
425 significantly smaller than that in the DG series. These observations could be related to
426 the fact that the initial fabric anisotropy intensity in the LG series is significantly greater
427 than that in the DG series (Table 1), providing stronger constraint on the orientation of
428 the shear strain. This hypothesis is also supported by observations in Fig. 9 (d) and (h),
429 where the oscillation amplitude of shear strain orientation in simulation DG-25-0 is
430 smaller than that in simulation DG-25-90, but similar to that in simulation LG-25-0,
431 with the initial contact normal fabric anisotropy α_{cin} of the three simulations being 0.075,
432 0.022, and 0.076, respectively (Table 1). These results indicate that unlike the
433 volumetric strain, which is independent of the bedding plane angle, the shear strain
434 induced by stress rotation is dependent on the bedding plane in terms of both magnitude
435 and orientation, thus being dependent on the initial fabric orientation. The magnitude
436 and orientation of shear strain, along with their dependency on initial bedding plane
437 angle are significantly influenced by the density of the material.

438 Similar to the volumetric strain, the deviatoric stress level also influences the shear
439 strain, as illustrated in Fig. 10. In both the DG series (DG-40-0, DG-25-0, and DG-10-

0) and LG (LG-40-0, LG-25-0, and LG-10-0) series of simulations with varying deviatoric stress, the stabilized maximum in-plane shear strain γ increases as the deviatoric stress q increases (Fig. 10 (a) and (c)). Interestingly, the oscillation amplitude of $\theta_{\varepsilon 1}$ decreases as the deviatoric stress increases (Fig. 10 (b) and (d)), which could again be related to the increase of initial fabric anisotropy intensity as deviatoric stress increases (Table 1).

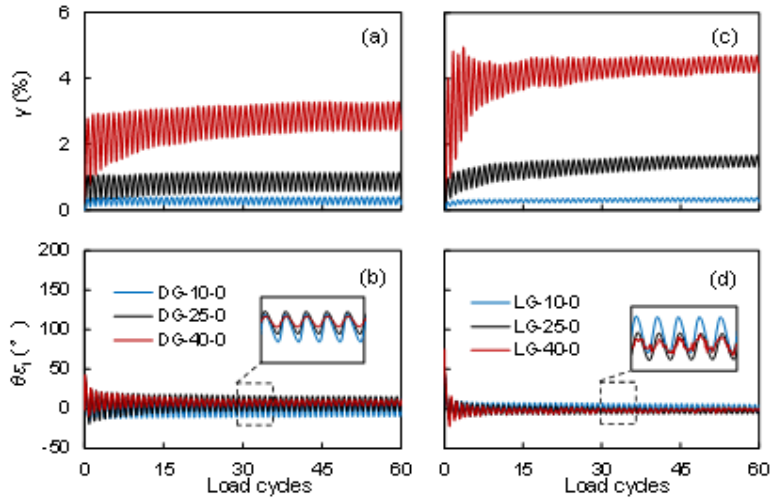

Fig. 10. Influence of deviatoric stress on shear strain: (a) maximum shear strain in series DG, (b) orientation of principal strain in series DG, (c) maximum shear strain in series LG, (d) orientation of principal strain in series LG.

5 Dilatancy under principal stress rotation

Detailed investigation into the relationship between volume change and shear deformation during stress rotation, which is referred to in this paper as dilatancy, can then be conducted based on the volumetric and shear strain measurements. As the strains exhibit two distinct stages of initial accumulation and eventual oscillation around stabilized values, dilatancy of both stages are analyzed.

Close-ups of the volumetric and maximum shear strain values during the first load cycle in the DG series of simulations with varying bedding plane angles are illustrated

458 in Fig. 11 (a) and (b), respectively. Fig. 11 shows that the volumetric and maximum
459 shear strain magnitudes during the first load cycle are almost completely independent
460 of the bedding plane angle and initial fabric orientation. This somewhat surprising result
461 has also been observed in laboratory principal stress rotation experiments by Xiong et
462 al. (2016) on Toyoura sand conducted using a hollow cylinder apparatus, as shown in
463 Fig. 12. Under stress rotation, the relative accumulation of volumetric strain to shear
464 strain is significantly greater than that under monotonic loading (Figs. 8 and 11). Hence,
465 the analysis of volumetric deformation and dilatancy should be a focus in investigating
466 the behavior of granular materials under stress rotation. It should also be pointed out
467 that Fig. 11 (a) and (b) have different vertical axis scales, the accumulated volumetric
468 strain during the first load cycle is about 0.15%, during which the accumulated shear
469 strain is also about 0.2%.

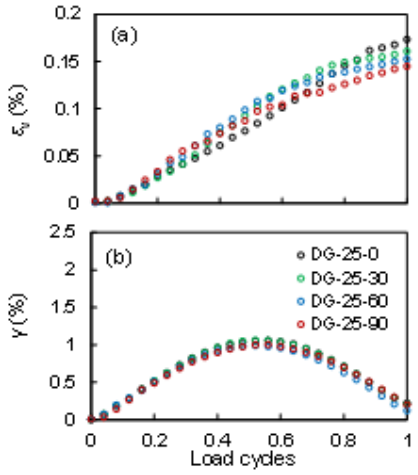

470

471 **Fig. 11.** Deformation in simulation series DG during the first load cycle: (a) volumetric strain, and
472 (b) maximum shear strain.

473 The dilatancy ratio ($\Delta\varepsilon_v/\Delta\gamma$) (also called simply dilatancy) during the first load cycle
474 in the DG simulation series is plotted in Fig. 13 against the orientation of the major
475 principal stress axis $\theta_{\sigma 1}$, which rotates from 90° to -90° (starting at the vertical direction

476 of 90°) during each cycle. During the first load cycle, the dilatancy ratio is always
477 positive for all the simulations in the DG series, echoing the contraction observed in
478 Fig. 11. For all four simulations with different bedding plane angles, the dilatancy peaks
479 when the major principal stress axis $\theta_{\sigma 1}$ is around 0°, which is the direction where the
480 specimen has been "compressed less" during initial consolidation under anisotropic
481 stress, and is perpendicular to contact normal fabric increment induced by consolidation
482 under anisotropic stress. The results in Figs. 11~13 indicate that the deformation of
483 granular material during the initial cycle of principal stress rotation is mostly dependent
484 on the orientation of the major principal stress axis in reference to that of the initial
485 major principal stress axis during anisotropic consolidation, and is almost independent
486 of the initial bedding plane angle and fabric anisotropy orientation.

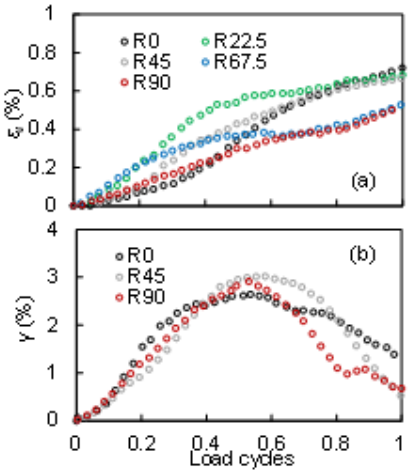

487

488 **Fig. 12.** Volumetric and shear strain during the first load cycle in laboratory principal stress rotation
489 experiments on Toyoura sand using a hollow cylinder apparatus: (a) volumetric strain, (b) maximum
490 shear strain. (The experiment results are obtained from data reported by Xiong et al. (2016). The
491 experiment IDs R0~R90 represent the bedding plane angle, which is the angle between the initial
492 major principal stress and the normal of the bedding plane)

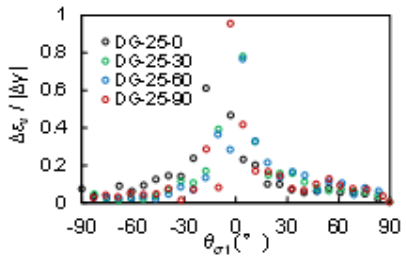

Fig. 13. Dependency of dilatancy rate on the orientation of principal stress during the first load cycle in simulation series DG. (The rotation direction for $\theta_{\sigma 1}$ is from 90° to -90° during each cycle).

During later load cycles, the deformation caused by principal stress rotation is observed to oscillate around a steady value. Fig. 14 shows the close-ups of the volumetric and maximum shear strain values during the 78th-80th load cycles in the DG series of simulations with varying bedding plane angles. Although the overall volumetric strain levels are similar for all four simulations as discussed in the previous section, clear phase difference in the periodic oscillation of the volumetric strain can be observed in Fig. 14 (a). The peak volumetric strain occurs at full cycles for DG-25-0, at half cycles for DG-25-90, at 5/6 for DG-25-30 and 2/3 cycles for DG-25-60. The maximum in-plane shear strain γ for the four simulations shows significant difference in value and slight phase difference during the 78th-80th load cycles (Fig. 14 (b)).

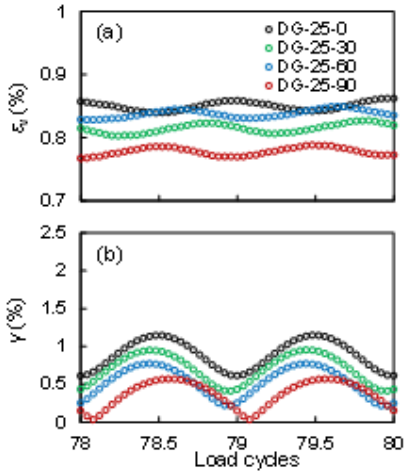

Fig. 14. Deformation in simulation series DG during the 78th-80th load cycle: (a) volumetric strain, and (b) maximum shear strain.

509 Fig. 15 (a) and (b) plot volumetric strain increment per increment of stress rotation
510 angle and per increment of max shear strain (the latter is also called the dilatancy ratio),
511 respectively, versus the angle between the major principal stress axis and the normal of
512 the bedding plane, namely $\psi - \theta_{\sigma 1} + 90°$. This reflects the relative orientation of both
513 stress and initial fabric anisotropy, unlike that in Fig. 13. During loading the rotation
514 direction for $\psi - \theta_{\sigma 1} + 90°$ is from 0° to 180°, while $\psi - \theta_{\sigma 1} + 90°$ initiates at 0°, 30°,
515 60°, and 90° for simulations DG-25-0, DG-25-30, DG-25-60, and DG-25-90,
516 respectively. Fig. 15 (a) clearly shows that the volumetric strain increment in terms of
517 increment of stress rotation angle in later load cycles is uniquely determined by the
518 angle $\psi - \theta_{\sigma 1} + 90°$. The dilatancy ratio in Fig. 15 (b) follows similar patterns as that in
519 Fig. 15 (a), but with more fluctuations. During the steady oscillation stage under
520 principal stress rotation, the dilatancy is zero when the either principal stress axis
521 coincides with the normal of the bedding plane. When the major principal stress axis
522 rotates from being aligned with the normal of the bedding plane to being perpendicular
523 to it, i.e. $\psi - \theta_{\sigma 1} + 90°$ rotates from 0° to 90°, dilatancy occurs. When the major principal
524 stress axis rotates from being perpendicular to the normal of the bedding plane to being
525 aligned with it, i.e. $\psi - \theta_{\sigma 1} + 90°$ rotates from 90° to 180°, contraction occurs. The results
526 in Figs. 14~15 indicate that the deformation of granular material after an adequate
527 number of cycles of principal stress rotation is dependent not only on the orientation of
528 stress itself, but also on the fabric anisotropy orientation, in terms of the particle
529 orientation fabric, which changes very little during stress rotation.

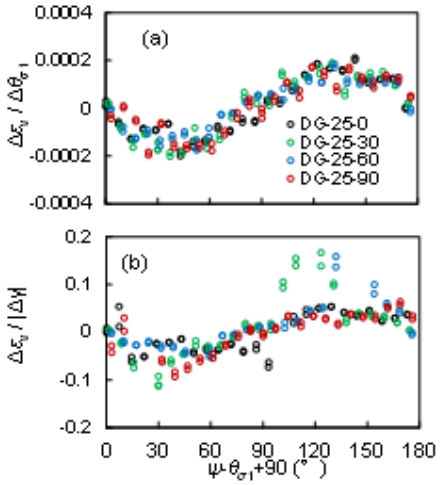

Fig. 15. Dependency of dilatancy on the angle between the orientation of principal stress and the initial bedding plane angle during the 78th-80th load cycles in simulation series DG: (a) volumetric strain increment rate (in terms of stress rotation angle $\theta_{\sigma 1}$); (b) dilatancy rate. (The rotation direction for ψ - $\theta_{\sigma 1}$ + 90° is from 0° to 180°).

Based on these evidence, we tentatively conclude that the orientation of stress in reference to its orientation during anisotropic consolidation and the angle between the stress and fabric anisotropy orientation both affect the dilatancy of granular material during stress rotation. During the initial loading stage, the influence of the orientation of stress in reference to its orientation during anisotropic consolidation dominates and causes substantial contraction, obscuring the role of initial fabric anisotropy orientation. As stress rotation continues, the influence of the orientation of stress alone gradually diminishes, and the influence of the angle between the stress and fabric anisotropy orientation becomes prominent, causing oscillations in the volumetric strain from dilative to contractive in each cycle. The volumetric strain results in Fig. 11 and Fig. 12 can provide some justification for the combination of these two different effects. Although the influence of the orientation of stress is overwhelmingly dominant, the volumetric strain during the second half of the first load cycle is slightly concave for the specimens with 0° bedding plane angle in Fig. 11 and Fig. 12. This means that the

549 volumetric strain is more to the contractive side when the major principal stress axis
550 rotates towards the normal of the bedding plane. However, the volumetric strain during
551 the same stage is slightly convex for the specimens with 90° bedding plane angle,
552 meaning that the volumetric strain is more to the dilative side when the major principal
553 stress axis rotates away from the normal of the bedding plane.

554 **6 Influence of initial fabric anisotropy intensity and loading history**

555 Having shown that the initial fabric anisotropy orientation influences the oscillation
556 of volumetric strain but has insignificant effect on its ultimate value in the stabilized
557 stage of stress rotations, it is natural to further investigate the influence of fabric
558 anisotropy intensity. Hence, an initially isotropic specimen is fabricated under
559 centripetal acceleration, consolidated under anisotropic stress, and then subjected to
560 stress rotation simulation (DC-25). The initial fabric anisotropy intensity for specimen
561 DC-25 is significantly smaller than its anisotropic counterpart DG-25-0 (Table 1)
562 deposited under gravity, although the two specimens have almost the same initial void
563 ratio. The slight initial contact normal fabric anisotropy intensity α_c in DC-25 is almost
564 completely induced by consolidation under anisotropic stress, increasing from 0.006 to
565 0.024 during consolidation. No change in the particle orientation fabric is observed
566 during consolidation of the specimen in DC-25, with the particle orientation fabric
567 anisotropy intensity α_p remaining constant at 0.008.

568 Fig. 16 compares the deformation in simulations DC-25 with that of DG-25-0. Fig.
569 16 (a) shows that the overall volumetric strain development in the two simulations are
570 very similar, reaching approximately the same ultimate stabilized value. However, a

major difference between them is that the initially isotropic DC-25 does not exhibit the oscillation of volumetric strain (Fig. 16 (a)), an expected behaviour considering the observed influence of the angle between the stress and initial fabric anisotropy orientation on such oscillation in initially anisotropic specimens. Hence, oscillations of dilatancy also does not exist for DC-25. The maximum shear strains for the two simulations are also different, with that of DC-25 being much smaller than that of DG-25-0 (Fig. 16 (b)). Fig. 17 plots the evolution of the contact normal fabric during stress rotation. Unlike its initially anisotropic counterpart in Fig. 5, the contact normal fabric orientation rotates in full circles along with the continuous rotation of the principal stress (Fig. 17 (b) and (d)) due to the fact that the slight initial anisotropy in DC-25 is purely induced by anisotropic consolidation. The particle orientation fabric is minimally altered by the principal stress rotation, and is not shown. The influence of initial fabric anisotropy intensity on the deformation of granular materials under stress rotation should be further analyzed, and it would be presumptuous yet to conclude that initial fabric anisotropy intensity does not affect the ultimate volumetric strain.

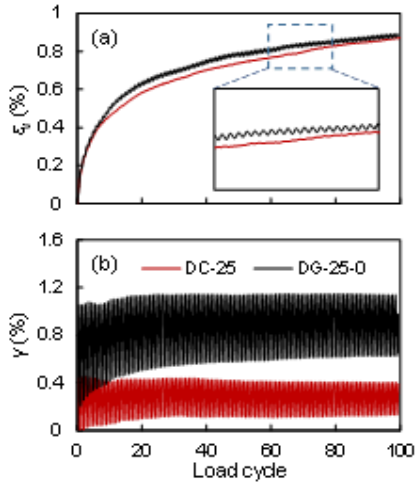

Fig. 16. Comparison of the deformation under continuous principal stress axis rotation in specimens

588 with and without significant initial fabric anisotropy (DG-25-0 and DC-25): (a) volumetric strain
589 during; (b) maximum shear strain.

590

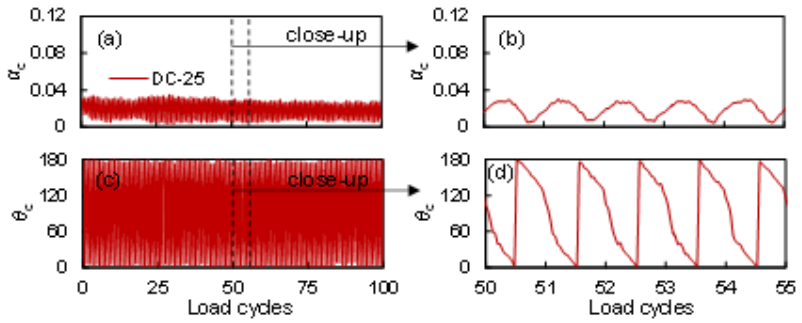

591

592 **Fig. 17.** Evolution of contact normal fabric during continuous cyclic principal stress rotation in
593 simulation DC-25: (a) contact normal fabric anisotropy intensity during 100 load cycles; (b) close-
594 up of contact normal fabric anisotropy intensity during 50~55 load cycles; (c) major principal
595 contact normal fabric orientation; (b) close-up of major principal contact normal fabric orientation
596 during 50~55 load cycles. (DC-25 is an initially isotropic specimen fabricated under centripetal
597 acceleration)

598 The possible influence of loading history on the deformation of granular material
599 under principal stress rotation is also investigated. A specimen (MR-25) that has
600 approximately the same initial contact normal and particle orientation fabric as those of
601 DG-25-0, but greater void ratio (0.1954 vs. 0.1818 as shown in Table 1), is
602 reconstructed from the specimen of LG-25-0 by applying biaxial stress histories. The
603 evolution of contact normal fabric, particle orientation fabric, and void ratio under
604 stress rotation in MR-25 is compared with those of DG-25-0 in Fig. 18. The specimen
605 of simulation DG-25-0 at load cycle 0, the initial state, has the same void ratio, contact
606 normal fabric, and particle orientation fabric as those in the specimen of MR-25 at load
607 cycle 21. This is highlighted in Fig. 18 by plotting the results of the two simulations on
608 two different horizontal axes, where cycle 0 in simulation DG-25-0 corresponds to
609 cycle 21 in simulation MR-25. From such a point on, if loading history has no influence
610 on the response of granular material under stress rotation, the two simulations should

become the same. However, although the fabric evolutions in the two simulations are almost identical (Fig. 18 (a)-(d)), the two simulations do not reach the same ultimate void ratio, the void ratio curves for the two simulations are eventually almost parallel to each other (Fig. 18 (e)). This means that loading history clearly has a strong influence on the deformation of granular material under principal stress rotation, and warrants further future analysis.

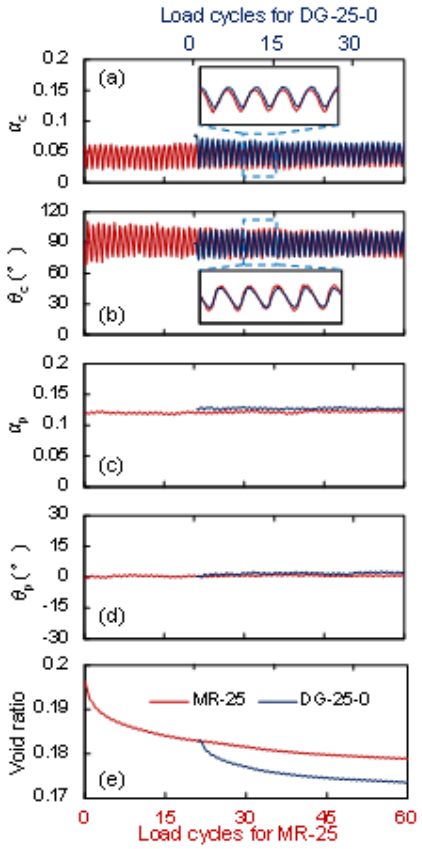

Fig. 18. The evolution of contact normal fabric, particle orientation fabric, and void ratio under 100 continuous principal stress axis rotation load cycles in simulations DG-25-0 and MR-25: (a) contact normal fabric anisotropy intensity; (b) major principal contact normal fabric orientation; (c) particle orientation fabric anisotropy intensity; (d) major principal particle orientation fabric orientation; (e) void ratio. Note the two simulations are plotted on different horizontal axis so that load cycle 0 in DG-25-0 coincides with load cycle 21.4 in MR-25 at which instant the two specimens have almost the same void ratio, contact normal fabric, and particle orientation fabric. (MR-25 is reconstructed from LG-25-0 after applying cyclic biaxial load history)

7 Conclusions

The purpose of this study is to investigate deformation behavior of granular material under continuous cyclic principal stress rotation, focusing on the volumetric strain, shear strain, dilatancy, and their relationship with fabric anisotropy. We found that the deformation induced by stress rotation is at least comparable to that induced by cyclic biaxial loading under the same level of deviatoric stress. The overall volumetric strain under stress rotation is contractive, irrespective of the initial void ratio of the material and the applied deviatoric stress ratio. However, the ultimate stabilized volumetric and shear deformation magnitudes are strongly influenced by the initial void ratio and applied deviatoric stress ratio, with looser specimen and greater deviatoric stress ratio generally resulting in larger deformation. For initially anisotropic specimens fabricated under gravity pluviation, the volumetric strain oscillates around a stabilized level after an adequate amount of load cycles.

The contact normal fabric oscillates significantly during stress rotation for initially anisotropic specimens, while the particle orientation experiences negligible change. The initial fabric orientation is shown to have little influence on the magnitude of volumetric strain, both during the initial load cycles and in the ultimate stabilized stage. In comparison, the value and orientation of the maximum shear strain is affected by the initial fabric anisotropy orientation, with the final maximum shear strain orientation tending to oscillate around the direction 45° to the bedding plane for looser specimens.

Using the volumetric and shear strain results, dilatancy that describes the relationship between volume change and shear deformation is also analyzed. The

results show that in early loading cycles, the dilatancy of granular material is dominated by the orientation of the major principal stress axis in reference to that of the initial major principal stress axis during anisotropic consolidation, causing contraction, and obscuring the influence of initial fabric anisotropy orientation. The contraction ratio during the initial load cycles is the greatest when the major principal stress is perpendicular to its initial orientation. For initially anisotropic specimens, as principal stress axes rotation continues, the influence of the orientation of stress gradually diminishes, and the influence of the angle between the stress and initial fabric anisotropy orientation becomes prominent, causing oscillations in the volumetric strain transitioning from dilative to contractive during each cycle. At the stabilized volumetric strain oscillation stage, the material dilates when the major principal stress axis rotates from the normal of the bedding plane to being perpendicular to it, and contracts when the major principal stress axis rotates from being perpendicular to the normal of the bedding plane to being aligned with it.

The influence of initial fabric anisotropy intensity and loading history on the deformation under principal stress rotation was also explored. A simulation on an initially isotropic specimen suggests that it is possible for specimens with the same void ratio but drastically different initial fabric anisotropy intensities to experience the same ultimate volumetric strain under stress rotation. The simulation on initially isotropic specimen does not exhibit the oscillation of volumetric strain that is observed for initially anisotropic specimens, while its contact normal fabric rotates in full circles following the rotation of stress. A simulation on a specimen that had been loaded under

cyclic biaxial prior to stress rotation shows that loading history has a strong influence on the deformation of granular material under principal stress rotation. The effects of initial fabric anisotropy intensity and loading history should be given further attention in future studies.

Acknowledgements

The authors would like to thank the National Natural Science Foundation of China (No. 51708332 and No. 51678346) for funding the work presented in this paper. Y. F. Dafalias acknowledges support by the European Research Council under the European Union's Seventh Framework Program (FP7/2007-2013) / ERC IDEAS Advanced Grant Agreement No. 290963 and partial support by the National Sciences Foundation (NSF) project CMMI-1162096. This paper is LLNL report LLNL-JRNL-744427.

References

Arthur J. R. F., Chua K. S., and Dunstan T. (1979) "Dense sand weakened by continuous principal stress direction rotation". *Geotechnique*, 29(1), 91-96.

Arthur J. R. F., Chua K. S., and Dunstan T. (1977) "Induced anisotropy in a sand". *Geotechnique*, 27(1), 13-30.

Bagi K. (1996) "Stress and strain in granular assemblies". *Mechanics of materials*, 22(3), 165–177.

Cai Y., Yu H. S., Wanatowski D., and Li X. (2012) "Noncoaxial behavior of sand under various stress paths". *Journal of Geotechnical and Geoenvironmental Engineering*, 139(8), 1381-1395.

Caillerie D. (1991) "Tenseur des contraintes dans un milieu granulair". Rapport d'activite´ Greco, 771–775. (In French)

Chang W. J. (2011) "Evaluation of undrained shear strains in multi-directional horizontal shaking". *Soil Dynamics and Earthquake Engineering*, 31(7), 906-920.

Cundall P. A. and Strack O. D. L. (1979) "A discrete numerical model for granular assemblies". *Geotechnique*, 29(1): 47-65.

Elata, D., and Berryman, J. G. (1996). "Contact force-displacement laws and the mechanical behavior of random packs of identical spheres". *Mechanics of Materials*, 24(3), 229-240.

Fu P. and Dafalias Y. F. (2011a) "Fabric evolution within shear bands of granular materials and its relation to critical state theory". *International Journal for Numerical and Analytical Methods in Geomechanics*, 35(18), 1918-1948.

Fu P. and Dafalias Y. F. (2011b) "Study of anisotropic shear strength of granular materials using DEM simulation". *International Journal for Numerical and Analytical Methods in Geomechanics*, 35(10): 1098-1126.
Fu P., Walton O. R., and Harvey J. T. (2012) "Polyarc discrete element for efficiently simulating arbitrarily shaped 2D particles". *International Journal for Numerical Methods in Engineering*, 89(5), 599-617.
Fu P. and Dafalias Y. F. (2015) "Relationship between void-and contact normal-based fabric tensors for 2D idealized granular materials". *International Journal of Solids and Structures*, 63: 68-81.
Gutierrez M., Ishihara K. and Towhata I. (1991). Flow theory for sand during rotation of principal stress direction. *Soils and foundations*, 31(4), 121-132.
Gutierrez M., Ishihara K., and Towhata I. (1993) "Model for the deformation of sand during rotation of principal stress directions". *Soils and Foundations*, 33(3), 105-117.
Hight D. W., Gens A., and Symes M. J. (1983) "The development of a new hollow cylinder apparatus for investigating the effects of principal stress rotation in soils". *Geotechnique*, 33(4), 355-383.
Iai S., Tobita T., and Ozutsumi O. (2013) "Induced fabric under cyclic and rotational loads in a strain space multiple mechanism model for granular materials". *International Journal for Numerical and Analytical Methods in Geomechanics*, 37(2), 150-180.
Ishihara K. and Towhata I. (1983) "Sand response to cyclic rotation of principal stress directions as induced by wave loads". *Soils and Foundations*, 23(4), 11-26.
Ishihara K. and Yamazaki F. (1980) "Cyclic simple shear tests on saturated sand in multi-directional loading". *Soils and Foundations*, 20(1), 45-59.
Jiang M. J., Li L., and Yang Q. (2013) "Experimental investigation on deformation behavior of TJ-1 lunar soil simulant subjected to principal stress rotation". *Advances in Space Research*, 52(1), 136-146.
Jiang M. J., Yu H. S., and Harris D. (2006) "Discrete element modelling of deep penetration in granular soils". *International Journal for Numerical and Analytical Methods in Geomechanics*, 30(4), 335-361.
Lashkari A. and Latifi M. (2008) "A non-coaxial constitutive model for sand deformation under rotation of principal stress axes". *International Journal for Numerical and Analytical Methods in Geomechanics*, 32(9), 1051-1086.
Li X. and Yu H. S. (2010) "Numerical investigation of granular material behaviour under rotational shear". *Géotechnique*, 60(5), 381-394.
Li X. S. and Dafalias Y. F. (2004) "A constitutive framework for anisotropic sand including non-proportional loading". *Geotechnique*, 54(1), 41-55.
Li X. S. (1997) "Rotational shear effects on ground earthquake response". *Soil dynamics and Earthquake Engineering*, 16(1), 9-19.
Matsuoka H., Koyama H., and Yamazaki H. (1985) "A constitutive equation for sands and its application to analyses of rotational stress paths and liquefaction resistance". *Soils and Foundations*, 25(1), 27-42.
Miura K., Miura S., and Toki S. (1986) "Deformation behavior of anisotropic dense sand under principal stress axes rotation". *Soils and Foundations*, 26(1), 36-52.

Miura K., Toki S., and Miura S. (1986) "Deformation prediction for anisotropic sand during the rotation of principal stress axes". *Soils and Foundations*, 26(3), 42-56.
Pradel D., Ishihara K., and Gutierrez M. (1990) "Yielding and flow of sand under principal stress axes rotation". *Soils and Foundations*, 30(1), 87-99.
Pyke R., Seed H. B., and Chan C. K. (1975) "Settlement of sands under multidirectional shaking". *Journal of the Geotechnical Engineering Division, ASCE*, 101(4), 370-398.
Satake M. (1982) "Fabric tensor in granular materials". Amsterdam: *Proceedings of the IUTAM Symposium on Deformation and Failure of Granular Materials*, 63-68.
Seed H. B., Martin G. R., and Pyke R. (1978) "Settlement of sands under multidirectional shaking". *Journal of the Geotechnical Engineering Division, ASCE*, 104(1), 27-44.
Symes M. J., Gens A., and Hight D. W. (1988) "Drained principal stress rotation in saturated sand". *Geotechnique*, 38(1), 59-81.
Taha M. R. and Shaverdi H. (2014) "Evolution of fabric under the rotation of the principal stress axes in the simple shear test". *Mechanics of Materials*, 69(1), 173-184.
Tejchman J. and Wu W. (2009) "Non-coaxiality and stress–dilatancy rule in granular materials: FE investigation within micro-polar hypoplasticity". *International journal for numerical and analytical methods in geomechanics*, 33(1), 117-142.
Theocharis A. I., Vairaktaris E., Dafalias Y. F., and Papadimitriou A. G. (2017) "Proof of Incompleteness of Critical State Theory in Granular Mechanics and Its Remedy". *Journal of Engineering Mechanics*, 143(2), 04016117.
Tokimatsu K. and Yoshimi Y. (1982) "Liquefaction of sand due to multidirectional cyclic shear". *Soils and Foundations*, 22(3), 126-130.
Tong Z., Fu P., Dafalias Y. F., and Yao Y. (2014) "Discrete element method analysis of non-coaxial flow under rotational shear". *International Journal for Numerical and Analytical Methods in Geomechanics*, 38(14), 1519-1540.
Tong Z. X., Zhang J. M., Yu Y. L., and Zhang G. (2010) "Drained deformation behavior of anisotropic sands during cyclic rotation of principal stress axes". *Journal of Geotechnical and Geoenvironmental Engineering*, 136(11), 1509-1518.
Towhata I. and Ishihara K. (1985) "Undrained strength of sand undergoing cyclic rotation of principal stress axes". *Soils and Foundations*, 25(2), 135-147.
Tsutsumi S. and Kaneko K. (2008) "Constitutive response of idealized granular media under the principal stress axes rotation". *International Journal of Plasticity*, 24(11), 1967-1989.
Vaid Y. P., Sayao A., Hou E., and Negussey D. (1990) "Generalized stress-path-dependent soil behaviour with a new hollow cylinder torsional apparatus". *Canadian Geotechnical Journal*, 27(5), 601-616.
Wan R. and Hadda N. (2015) "Plastic deformations in granular materials with rotation of principal stress axes". In: *Bifurcation and Degradation of Geomaterials in the New Millennium*, Springer International Publishing, 305-310.

Wang R., Fu P., Zhang J. M., and Dafalias Y. F. (2016) "DEM study of fabric features governing undrained post-liquefaction shear deformation of sand". Acta Geotechnica. 11 (6), 1321-1337.
Wang R., Fu P., Tong Z. X., Zhang J. M., and Dafalias Y. F. (2017a) "Strength anisotropy of Circular-Particle Deposits". *International Journal for Numerical and Analytical Methods in Geomechanics*, 41(17), 1758–1778.
Wang R., Fu P., Zhang J. M., and Dafalias Y. F. (2017b) "Evolution of various fabric tensors for granular media towards the critical state". *Journal of Engineering Mechanics*, 143(10), 04017117-1-9.
Wijewickreme D., Vaid Y. P. (1993) "Behaviour of loose sand under simultaneous increase in stress ratio and principal stress rotation". *Canadian Geotechnical Journal*, 30(6), 953-964.
Xiong H., Guo L., Cai Y., and Yang Z. (2016) "Experimental study of drained anisotropy of granular soils involving rotation of principal stress direction". *European Journal of Environmental and Civil Engineering*, 20(4), 431-454.
Yan J. J., Zhou J., Gong X. N., and Cao Y. (2015) "Undrained response of reconstituted clay to cyclic pure principal stress rotation". *Journal of Central South University*, 22, 280-289.
Yang Y. and Yu H. S. (2013) "A kinematic hardening soil model considering the principal stress rotation". *International Journal for Numerical and Analytical Methods in Geomechanics*, 37(13), 2106-2134.
Yang Z. X., Li X. S., and Yang J. (2007) "Undrained anisotropy and rotational shear in granular soil". *Geotechnique*, 57(4), 371-384.
Yao, Y. P, Tian, Y and Gao, Z. W. (2017) "Anisotropic UH model for soils based on a simple transformed stress method". *International Journal for Numerical and Analytical Methods in Geomechanics*, 41, 54-78.